OH-Initiated Oxidation of Toluene. 2. Master Equation Simulation of Toluene Oxide Isomerization†

Terry J. Frankcombe*

Leiden Institute of Chemistry, Gorlaeus Laboratories, Leiden University, P.O. Box 9502, 2300 RA Leiden, The Netherlands

Sean C. Smith‡

Centre for Computational Molecular Science, University of Queensland, St. Lucia, Queensland 4072, Australia

Received: October 30, 2006

In this work we continue our investigation of the toluene−OH−O_2 system. We describe master equation modeling of the isomerization of toluene oxide, focusing on the formation of the cresols. A 15 isomer model is used. Simulations of both thermally activated processes and photolysis processes are described. In accord with experiment, it is found that photolysis with a high-energy light source should be expected to give a high yield of the thermal distribution of cresol products (dominated by the para isomer). Photolysis with a low-energy light source, on the other hand, favors formation of the thermally disfavored ortho isomer. Though the 15 isomer system is potentially an excellent test bed for the development of scalable master equation solution methods, existing scalable solution methods were found to fail on this system.

1. Introduction

Toluene is one of the major aromatic atmospheric pollutants. Hence understanding the atmospheric chemistry of toluene of great importance. The main route for degradation of atmospheric toluene is via reaction with OH radicals.[1−6] In the preceding paper[7] (henceforth referred to as paper 1) we used quantum chemistry methods to explore the reaction of toluene with OH radicals (which has been the subject of previous theoretical investigations[4,8−11]) and the less studied further reaction with O_2. Rather than looking for stable O_2 addition products, the reaction scheme investigated was based on that proposed by Klotz et al.,[3] in which O_2 serves primarily as a hydrogen acceptor.

Although Klotz et al. proposed direct formation of the cresols observed during photolysis of toluene oxide, paper 1 identified a number of ketone structures appearing on the minimum energy paths from the toluene oxide isomers to the cresols. These structures lay significantly higher in energy than the cresols that can form from them, with energy barriers to cresol formation being lower than the barriers that must be surmounted to form the ketones from the toluene oxides. Though one would normally expect that such a situation would lead to rapid isomerization to the cresol products, these ketone structures are candidates for the unidentified carbonyl photolysis products observed by Klotz et al.

Networks of interconverting species such as those identified in paper 1 can be studied using master equation modeling. The energy-grained master equation (EGME) can be formulated for such *multiwell* problems to include explicit consideration of non-equilibrium populations and collisional effects.[12−14] Recently we have developed several methods that are designed to exhibit linear scaling characteristics, with the computational time required to solve the master equation being proportional to the number of isomers being modeled.[15,16] Part of the motivation of this work was to provide additional test cases for such methodological development, which requires well-characterized large networks of isomers.

To model the experiments of Klotz et al., and to establish a good test case for scalable EGME method development, the isomerization of toluene oxide was chosen. This system provides a well-defined network of reactions incorporating the toluene oxides, methyloxepins, cresols and other ketone intermediates that were described in paper 1 and that would have been present in the experiments of Klotz et al.

2. Isomerizing Network Model

Fifteen species were included in the modeling performed in the work described in this paper. The species were selected from those identified in paper 1 on the basis of modeling the photolysis of toluene oxide and its methyloxepin isomers. The reaction network is outlined in Figure 1, and the energies along the minimum reaction path are shown in Figure 2. The labels used are those assigned in paper 1. Figure 2 is similar to Figure 3 of paper 1, with the methyloxepin isomers **6**−**8** having been added in the figure in this paper. The experiments of Klotz et al. started with toluene-1,2-oxide (**3**), which they considered to be an equilibrium mixture of **3** and its methyloxepin isomer **6**. Their observed products were the cresols **9**−**11**.

The geometric, energetic and vibrational parameters for each of the 15 species were taken to be those reported in the Supporting Information accompanying paper 1. The vibrational densities of states for the stationary points in the reaction scheme were calculated in the harmonic approximation. A scaling factor of 0.9670 was uniformly applied to the harmonic frequencies and zero point energy contributions from paper 1. Harmonic RRKM theory[17] was used to determine the microscopic rate constants for the interconversions between the isomers.

† Part of the special issue "James A. Miller Festschrift".

* Corresponding author. E-mail: T.Frankcombe@chem.leidenuniv.nl.
‡ E-mail: S.Smith@uq.edu.au.

10.1021/jp067113a CCC: $37.00
Published on Web 01/18/2007

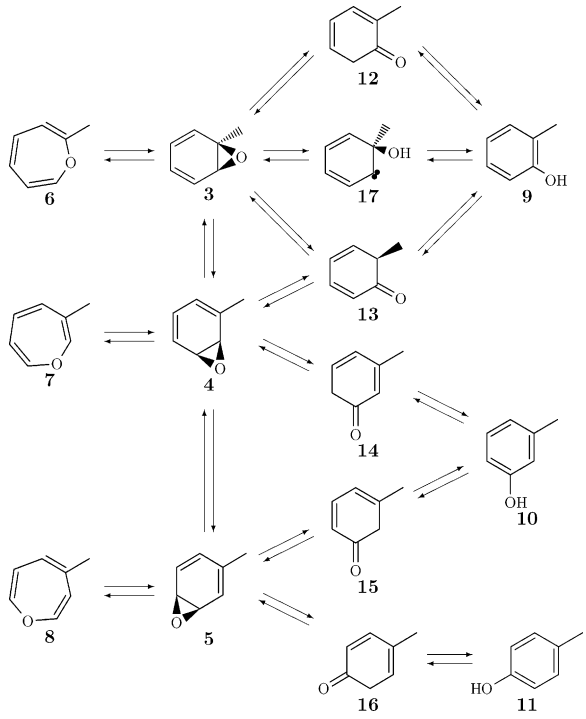

Figure 1. Network of modeled isomers accessible from toluene oxide. The first column (**6**−**8**) contains methyloxepins, the second column (**3**−**5**) contains toluene oxides, the majority of the third column (**12**−**16**) is composed of methylcyclohexadienone ketones and the final column (**9**−**11**) contains cresols. See paper 1[7] for details.

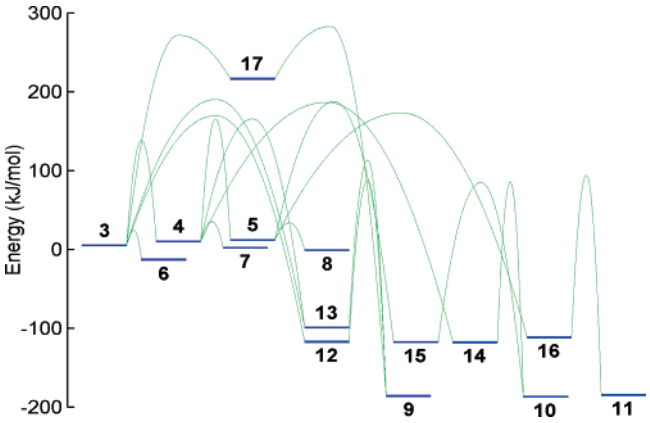

Figure 2. Minimum energy pathway of the reaction scheme shown in Figure 1.

The energy graining for the EGME description was done with an energy grain size of 1.196 kJ/mol (approximately 100 cm^{-1}). Energies up to 598 kJ/mol above the zero point energy of toluene-1,2-oxide were included. Hence toluene-1,2-oxide was described by 500 energy grains and the species with the lowest zero point energies, the cresols, were described by up to 660 energy grains. The total state space for the 15 isomers was 8320 grains.

The EGME treatment requires a specification of the collisional energy transfer (CET) processes for each modeled species. In the absence of detailed information for all the modeled species, the CET properties of all the species were taken to be the same as those measured for toluene. The CET kernel function was taken to be the accurate parametric exponent model of Lenzer et al.[18,19] in which the deactivating collisions are described by

$$P(E|E') \propto \exp\left[-\left(\frac{E'-E}{C_0 + C_1 E'}\right)^Y\right] \qquad (1)$$

where C_0, C_1 and Y are parameters, typically with $Y \approx 0.8$. Transition probabilities for activating collisions ($E' < E$) were determined by detailed balance and the probabilities were explicitly normalized.[17,20] This kernel exhibits a significantly different shape to the popular exponential down model in which the average energy transferred in deactivating collisions, $\langle \Delta E \rangle_{down}$, is usually taken to be independent of initial energy E' despite experimental evidence to the contrary. In the present case, to simulate toluene dilute in air, the parametric exponent model parameters were taken as those for toluene in CO_2 from Lenzer et al.[19] The collision frequency was taken as the Lennard-Jones collision frequency with the parameters taken from the N_2 values of Hippler, Troe and Wendelken.[21]

3. Master Equation Methods

The EGME is well-known,[12,14,17,20,22,23] and so it will not be described in detail here. Usually the EGME matrix **A** can be symmetrized by a simple transformation to yield a symmetric matrix **B**. Solution of the EGME comes down to solving the differential equation (DE)

$$\frac{dy}{dt} = \mathbf{B}y \qquad (2)$$

as a function of time t for some suitable initial transformed population $y(t=0)$. Two common ways to solve eq 2 are by direct integration using a "stiff" integrator and by spectral solution, where the matrix exponential of the formal solution to eq 2 is expanded in terms of the eigenvalues and eigenvectors of **B**. A number of variations of these methods have been directly compared in a previous paper.[14]

The EGME matrix for multiwell problems (describing more than one energy grained species) is a block matrix, with dense blocks on the main diagonal describing collisional processes and reactive loss and diagonal blocks off the main diagonal describing interconversion between the species. Bimolecular reactions can also be accommodated.[12,24]

In a recent series of papers[15,16] we developed two new methods designed to be extendable to networks of reacting species, such as the present case. These methods are designed to require a computational effort scaling linearly with the number of species being described, rather than the cubic scaling of other spectral and integration methods. These methods, a stiff integration method and a shift-invert Lanczos method, are based around inverting the master equation matrix (or a matrix simply derived from it) using a pre-conditioned GMRES iteration. For the stiff integrator the matrix needing to be inverted is $\mathbf{I} - \gamma\mathbf{B}$, where γ is a time-dependent scalar determined by the integration algorithm, whereas the shift-invert Lanczos method requires solutions of linear systems involving $\mathbf{B} - \sigma\mathbf{I}$, where σ is the applied constant shift. The success of the methods relies on the availability of a quality and easily inverted approximation to the EGME matrix, namely that provided by the diffusion approximation.[25] In this approximation the dense blocks on the diagonal of the EGME matrix collapse to tridiagonal blocks, wherein a simple permutation brings the matrix into easily inverted banded or banded arrowhead form, suitable for use as a preconditioner to the GMRES iteration. These methods are highly successful in solving multiwell EGMEs based on the reaction of singlet methylene with acetylene to form propargyl via a number of intermediates.[15]

Although the new scalable methods were applied in this work, the bulk of the calculations described herein were performed using the traditional cubic scaling methods. For the spectral solution, complete eigendecompositions of the symmetrized

EGME matrix were determined using the Dsyev routine from Lapack.[26] It was soon discovered that the nature of the EGME matrix for the present case was such that double precision calculations (with unit roundoff of the order of 10^{-16}) did not result in a sufficiently accurate eigen decomposition to reliably propagate an initial toluene-1,2-oxide population, even at 2000 K and 500 kPa. Quadruple precision calculations (with unit roundoff of the order of 10^{-34}) could reliably describe the kinetics of the system down to 300 K. It is unclear which aspect of the current system leads to the observed requirement of a high precision description. Once a complete eigen decomposition of the EGME matrix had been determined any number of different initial populations could be propagated in time with significantly reduced computational cost.

Numerical integration of eq 2 was also performed using the Lsoda integrator.[27] Although the direct integration results were useful to confirm that the quadruple precision spectral solution results were accurate down to 300 K, even in quadruple precision the direct spectral decomposition required less computational effort to solve the problem than the numerical integration of the EGME DE. Thus the result described below were calculated using the quadruple precision spectral decomposition.

4. Modeling Results

4.1. Thermal Decomposition of Toluene-1,2-oxide. Energy-resolved populations of the 15 isomer system were propagated from $t = 0$ to $t = 10^5$ s (about 28 h). The initial population was taken as a thermal distribution of toluene-1,2-oxide (species **3** of Figures 1 and 2). The system was modeled for temperatures from 300 to 2000 K. The whole temperature range was modeled for a pressure of 500 kPa. A selection of the calculated population profiles are shown in Figure 3. The population of the high energy isomer **7** has been excluded as it was only present in appreciable amounts at 2000 K.

Like in previously published multiwell master equation simulations,[13] the observed population profiles can be rationalized in terms of a number of competing processes involving subsets of the modeled species. These shall be described with reference to the 1000 K populations, shown in Figure 3a. At short times very rapid decomposition of the toluene-1,2-oxide population initially above the reaction barriers lead to excited (non-thermal) populations of all of the other isomers. Controlled by competition between the various microscopic rates, the populations of all the other isomers grew rapidly. The equilibrium between the populations of the nascent toluene oxides **4** and **5** and the corresponding methyloxepins **7** and **8** was quickly established, with the lower rate of formation of **5** allowing the **5** ⇌ **8** equilibrium to be established sooner than the **4** ⇌ **7** equilibrium. **3** ⇌ **6** equilibrium took significantly longer to become established due to the initial **3** population below the reaction barrier, requiring collisional activation to become involved in the equilibrium. Due to the finite supply of reactant in this simulation, at times between 10^{-9} s and 10^{-8} s the rate of formation of the ketone intermediates **12**−**16** from the toluene oxides dropped lower than the rate of their decomposition to the cresols **9**−**11** and their populations began to drop. By 10^{-7} s collisional activation of the initial population of **3** was bringing reactant population above the reactive barriers, effectively increasing the available reactant and allowing the rate of formation of the ketone intermediates to again rise above the rate of cresol formation, leading to a rise in the intermediate population. Soon thermodynamic equilibrium between the toluene oxides, methyloxepins and ketones became established, leading to the intermediate approximate steady state at times

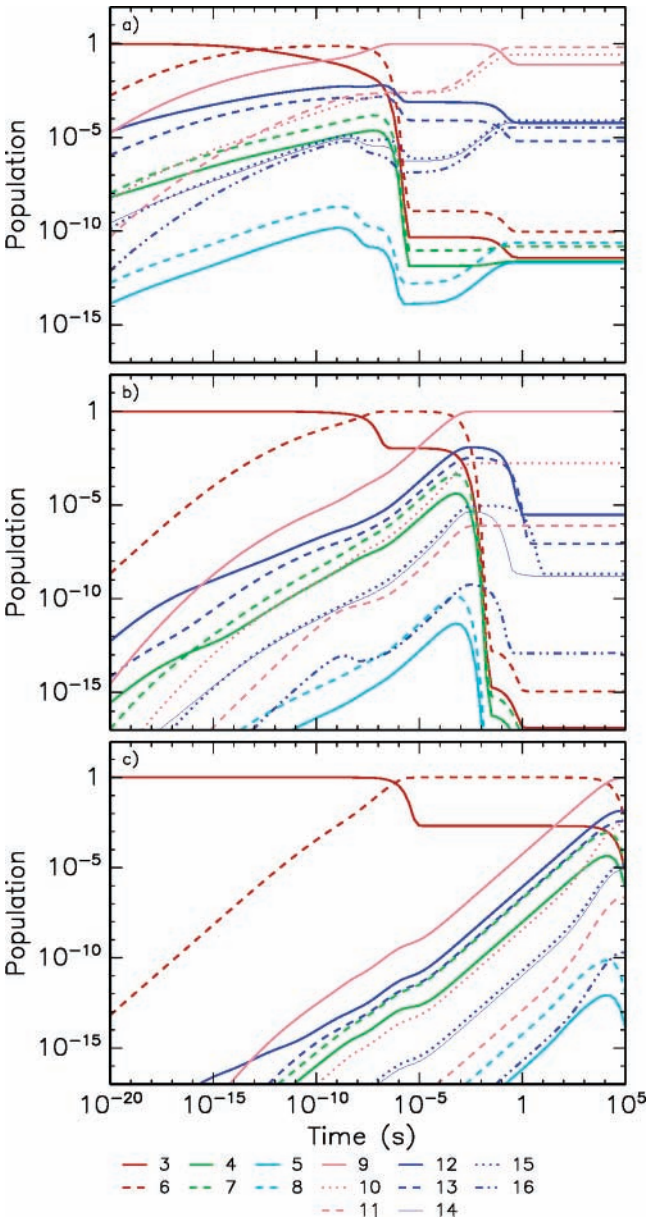

Figure 3. Calculated population profiles for the thermal decomposition of toluene-1,2-oxide (**3**) at 500 kPa: (a) 1000 K; (b) 600 K; (c) 400 K.

shorter than 10^{-6} s. During the establishment of this equilibrium, *o*-cresol **9** formed rapidly via the intermediates **12** and **13**. By the time the oxide−oxepin−ketone equilibrium was established, significantly more than 99% of the total population lay in this isomer. This did not represent the long-time equilibrium of the system, though the branching fractions to the reactant and intermediate isomers were approximately correct. The zero point energies of the three cresols are similar and lie significantly lower than the other species in the system (Figure 2). However, the calculated partition functions of these three isomers were such that thermodynamic equilibrium favors *p*-cresol **11**, with *o*-cresol **9** being the least favored cresol isomer. Indeed, the calculated equilibrium ortho to para ratio of the cresols was found to be 21% at 300 K, dropping to 15% at 500 K and 12% at 1000 K. The calculated 1000 K populations began to move toward this equilibrium after 10^{-4} s. At times of the order of 1 s this long time equilibrium had become established, along with the corresponding shift in the populations of the ketone intermediates and toluene oxides/methyloxepins in the lower half of the reaction scheme of Figure 1.

These same processes were of course evident in the calculated populations at 600 K, though the time scales changed. The reduced temperature dramatically reduced the initial population at high energies, thus dramatically reducing the initial formation rates of the other isomers from **3**. The reduced temperature enhanced the effect of the differences in the barrier heights of the competing pathways for toluene-1,2-oxide decomposition, meaning that the equilibrium between **3** and its methyloxepin isomer **6** could become established long before reactive loss to the rest of the system became significant, allowing the establishment of a near steady state in the populations of these two isomers from times shorter than 10^{-6} s to times approaching 10^{-4} s. The small differences in the barrier heights for isomerization between the toluene oxides and conversion to the ketone intermediates also became evident with the lower reaction rates. The establishment of near equilibrium between the six toluene oxide/methyloxepin species, before further reaction to the ketone intermediates, became evident at times shorter than 10^{-2} s. Shortly thereafter equilibrium was established among the oxide−oxepin−ketone species, reflected in the temporary dramatic slowing of the rate of decrease of the populations of the six oxide/methyloxepin isomers just after $t = 10^{-2}$ s. Reaction to form the cresols continued for a short time. At this reduced temperature the time scale for the establishment of the long-time equilibrium was longer than the simulation time. (At 700 K, not shown in Figure 3, the beginning of the shift away from the intermediate-time equilibrium, but not the establishment of the long-time equilibrium, did lie within the simulation time scale at $t < 10^5$ s.)

At 400 K (Figure 3c) the conversion rate from the initial population became so slow that the only equilibrium obviously established within the simulation time were those between the toluene oxides and their corresponding methyloxepins. The largely collision-independent equilibria involving the nascent toluene oxide isomers were once again established quickly. The **3** ⇌ **6** equilibrium was established later than in the 600 K case, but the comparative delay was much shorter than that for significant loss to other isomers (which only occurred after around 10^3 s). This is indicative of the dependence of the time scale for collisional activation on the height of the relevant energy barrier.

Modeling was performed for pressures of 300 and 100 kPa at temperatures of 500 and 1000 K. This factor of 5 change in the pressure (from the 500 kPa modeling described above) did not dramatically effect the observed evolution of the populations of the isomers. At times shorter than 10^{-7}−10^{-9} s, where the dynamics was controlled exclusively by the competition between microscopic rates with no significant collisional effect, the population profiles were necessarily unaffected. At longer times, lowering the pressure simply shifted the evolution of the populations to marginally longer times. The overall shape of the population profiles and the relative populations in the plateaux in the profiles remained the same for this pressure range.

In all cases equilibrium between **3** and **6** was established before the majority of the combined **3** and **6** population had reacted to form other isomers. Thus one could estimate the thermal lifetime of toluene oxide from the time taken for the **3** and **6** population (effectively just the **6** population, favored by equilibrium) to drop to 1/e ≈ 0.37. Klotz et al. estimated a room temperature thermal lifetime around 330 min, on the basis of the observed formation rate of *o*-cresol. In the 300 K simulations performed in this work, the methyloxepin (**6**) population, once formed by isomerization from **3**, did not drop significantly

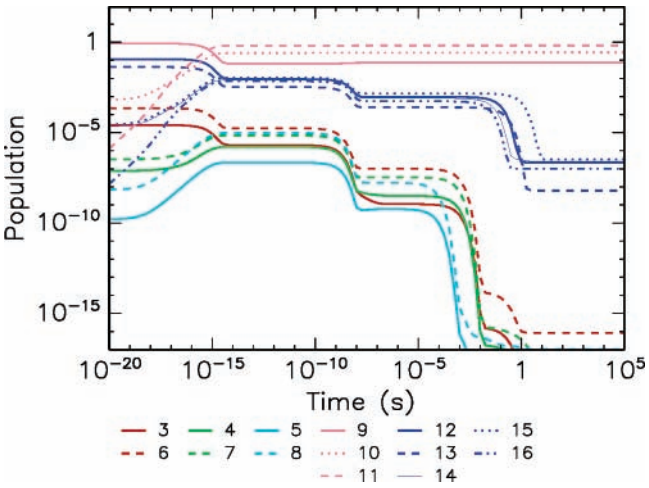

Figure 4. Population profiles calculated at 600 K and 500 kPa for the evolution of an initial 2-methyloxepin (**6**) population at 470 kJ/mol (254 nm).

before the simulations were finished at $t = 10^5$ s ≈ 28 h. Thus the room temperature thermal lifetime suggested by these simulations was significantly greater than the 5−6 h suggested by Klotz et al. The lifeline could be calculated at 400 K and above, yielding values of 4.6 h at 400 K, dropping to less than 7 ms at 500 K and continuing to drop rapidly with increasing temperature. In the calculated population profiles there was no evidence that, at the low temperatures considered by the experiment, the rate of appearance of *o*-cresol is not a good indicator of the rate of decomposition of toluene oxide/methyloxepin.

4.2. Modeling of Photolysis. To model the photolysis experiments of Klotz et al., initial populations composed of a microcanonical ensemble of a single reactant (approximated by a single non-zero grain of the initial population vector) were propagated in the same way as described above for the thermally distributed initial populations. Initial populations of **3** and **6** were investigated, at 332 kJ/mol and 470 kJ/mol. These energies correspond to the 360 and 254 nm maximum intensity wavelengths of the photolysis lamps used by Klotz et al. Given the qualitative insensitivity to pressure of the thermally activated simulations discussed above, only simulations at 500 kPa were performed.

Due to the linearity of the EGME DE, one could easily construct time dependent populations for an initial population of a mixture of **3** and **6** by a simple weighted sum of the separate time-dependent populations. However, little difference was found between the simulations with excited populations in each of the two isomers, due to the speed with which the two isomers establish equilibrium when collisional activation is not required. For the higher energy initial populations, the time-dependent population profiles were virtually indistinguishable for times $t > 10^{-15}$ s. For the lower energy initial populations the differences in the population profiles were limited to some minor changes in the timing of the establishment of steady states and the details of the population levels within these steady states. Thus only results from the initially excited 2-methyloxepin (**6**), the dominating isomer at pre-photolysis equilibrium, will be discussed here.

A sample population profile is shown in Figure 4. One of the most striking features of the populations calculated from the high energy initial population was the lack of dependence of the cresol populations on temperature, reflecting the very weak temperature dependence of the thermal equilibrium

populations of the different cresols, particularly at elevated temperatures. The populations of all of the isomers were independent of temperature for simulation times less than around 10^{-8} s, where collisional processes started to play a role. Figure 4 indicates that before this time the system had passed through a pair of near steady states. Like the thermally activated case discussed above, at short times population flows from the initial isomer to the other isomers under the control of the microscopic rate constants. A near steady state is reached quickly (at times shorter than those shown in Figure 4) in which most of the isomers are in equilibrium. In this regime population continues to flow into the lowly populated cresol isomers until they come into kinetic equilibrium in the readjustment around 10^{-15} s. At times shorter than 10^{-9} s collisional relaxation of the populations (until that time centered on the 470 kJ/mol initial energy) favors the cresols, with the redistribution between the isomers occurring quickly under the influence of the fast, high-energy kinetics. The timing of the subsequent redistribution of population into the cresols to form the thermally distributed population (occurring later than 10^{-5} s in Figure 4) was temperature dependent. Lower temperatures lead to later redistribution and lower residual non-cresol population. The ordering of the magnitudes of the relative residual populations within the groups of isomers (e.g., within the ketone intermediates) remained largely independent of temperature, controlled as it was by local equilibria within the groups. Being less thermodynamically favored, the redistribution of population out of the toluene oxides and methyloxepins occurred faster and more dramatically than out of the ketones. At room temperature the temperature-dependent shift of population out of the ketone intermediates to achieve thermal equilibrium occurred at times much greater than the simulation time. Thus one would expect that the experimentally accessed populations were from this temperature-independent region. After the initial reshuffling of population between the cresols around 10^{-15} s, the magnitudes of the populations of these isomers meant that the later temperature-dependent redistributions of population from the other isomers (at $t > 10^{-8}$ s) did not significantly alter the cresol populations, yielding their observed weak temperature dependence.

The population profiles resulting from the initial population at 332 kJ/mol were qualitatively similar to those discussed above for the high energy initial population, with the notable exception of the cresol populations. Initially, the non-reactant isomers formed under the control of the microscopic rate constants, leading to a temperature-independent near steady state with growing populations of meta and para cresol isomers **10** and **11**. However, due to the much lower rate of reaction for the lower energy population, collisional processes were starting to act at the time scales at which the cresols [initially dominated by *o*-cresol (**9**)] were kinetically equilibrating with the rest of the system. This resulted in much stronger and more complex dependence of the cresol populations on the temperature of the system, shown in Figure 5. The thermalization of the cresol populations favored retention of population in the *o*-cresol isomer until the much later times at which thermodynamic equilibrium could become established within the whole system. As discussed above, at lower temperatures the thermal equilibration occurred at very long times, of the order of days or longer. Thus this modeling suggests that at experimentally accessible time frames at room temperature the observed cresol branching fractions are those of the non-equilibrium populations determined by competition between thermalization of the rapidly formed *o*-cresol population and the kinetically favored transfer to *p*-cresol.

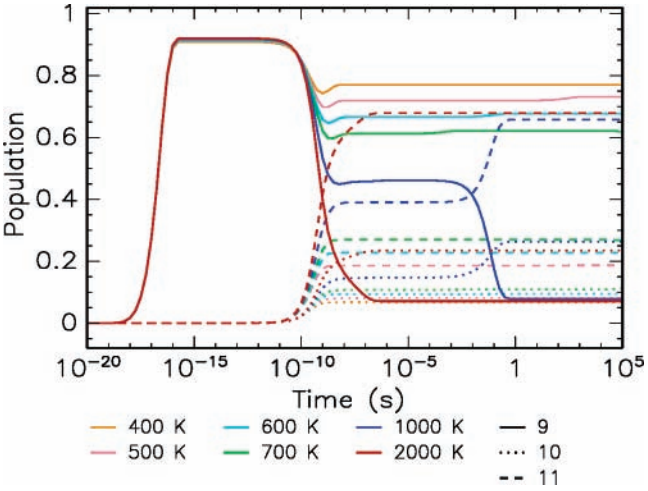

Figure 5. Population profiles of cresol isomers calculated at 500 kPa for the evolution of an initial 2-methyloxepin (**6**) population at 332 kJ/mol (360 nm). (Note the non-logarithmic scale of the *y*-axis.)

4.3. Initial Exploration with Scalable Methods. One of the motivations for this work was to provide a test bed for scalable master equation solution methods, such as those developed by us recently and described in section 3.[15,16] These methods have demonstrated excellent utility in the previous application to the $^1CH_2 + C_2H_2$ reaction.

The current 15 isomer toluene oxide system seems to be a difficult test case. Even at 2000 K, quadruple precision arithmetic was required for a direct spectral solution and numerical integration of the EGME DE required significantly more time steps than expected. The shift-invert Lanczos method that has proven effective in the past[14] failed for non-conservative subsystems.

Numerical integration using diffusion-preconditioned GMRES iterative inversion was applied to small subsets of the 15 isomer network. For short simulation times the integration with iterative inversion worked nearly identically to the standard integration with explicit inversion. At $t = 10^{-10}$ s the Lsoda integration stepsize stopped increasing with simulation time, meaning that the number of matrix-vector products (MVPs) and system solves required to integrate the populations increased dramatically. Although the origin of the failure of the scalable integration method has not been investigated fully, there is evidence that points to an unexpected propagation of error into the integrator: First, the convergence criterion for the GMRES iterative inversion was set to a relative residual norm of 10^{-15}, which was readily achieved. Although this is similar to the quality of solution one would expect from the explicit factorization and back-solution applied in the standard numerical integration, this gives no control over variations in the accuracy of the solution vector in different energy regions. Iterative iteration could conceivably give a solution vector with non-zero error components corresponding to an ill-conditioned energy region, a property reflecting the structure of the EGME matrix. Second, in the iterative solution case numerical noise was observed to grow in the small magnitude regions of the calculated populations for times leading up to the $t = 10^{-10}$ s at which the method diverged. Similar noise was observed in the explicit inversion case, but this noise died out before $t = 10^{-10}$ s. Third, implementing the entire numerical integration and preconditioned iterative inversion scheme in quadruple precision resulted in a more successful (but still failing) method. A 20% reduction in the required number of MVPs for simulation times up to $t = 10^{-10}$ s was observed. However, by $t = 10^{-4}$ s the number of

MVPs had caught up with the number required for the explicit inversion integrator, and rose quickly. Repeating this high precision calculation with the iterative inversion relative residual norm convergence criteria tightened to 10^{-20} resulted in exactly the same number of MVPs for any particular simulation time.

Although the onset of the integration difficulties being at $t = 10^{-10}$ s, around the time that collisional processes become important in this problem, may implicate the initial-energy dependent CET kernel used in this work, repeating the integrations with a standard exponential-down kernel gave the same results. Investigations into the cause—and hence circumvention—of the failure of the scalable integration method are ongoing.

5. Discussion and Conclusion

Although the modeling performed in this work was based on stationary points characterized with rigorous quantum chemistry calculations, a number of possible deficiencies can be identified. Treating all motions within the various isomers as harmonic vibrations rather than, for example, hindered rotation of methyl fragments or pseudorotation of ring modes could lead to significant error in the calculated densities and sums of states. Using RRKM theory to describe the reactions as occurring strictly along the minimum energy pathways could lead to significant error in the description of the rate constants. This may particularly be the case for the toluene oxide ⇌ ketone ⇌ cresol reactions, in which the minimum energy pathways have a hydrogen atom migrating from one carbon site to another, then effectively turning around and coming back. One could reasonably expect that the hydrogen motion in such a process would be somewhat truncated when there was significant amounts of excess energy in the system.

Treating the initial population in the modeling paralleling the photolysis experiments as microcanonical populations is not a particularly accurate representation of the expected initial population, given the chromatic nature of the photolysis lamps used and the thermal distribution of the reactant population before excitation. However, we feel that our treatment is a reasonable approximation, particularly with regard to elucidating the differences between the behavior of the system when excited with different frequency sources and between these and thermally activated decomposition.

The present modeling of the initially excited 2-methyloxepin population yields particular insight into the cresol formation observed by Klotz et al.[3] The modeling revealed that one should expect high-energy photolysis to yield initially a high population of *o*-cresol that evolves into the thermal cresol distribution, which was calculated to give [*p*-cresol] ≫ [*m*-cresol] ≫ [*o*-cresol]. Though the time scales are different, this is exactly what was observed in the experiments, with an initial relatively large *o*-cresol yield and smaller but growing *m*-cresol and *p*-cresol populations. Low-energy photolysis, on the other hand, gives *o*-cresol forming much more rapidly than the thermal decomposition rate, then being "frozen in" by thermalization of the *o*-cresol population before the other cresol isomers can form via the ketone intermediates. This readily explains why only *o*-cresol was observed in the low-energy photolysis experiments of Klotz et al.

Though the ketone intermediates identified in paper 1 could be considered potential candidates for the major carbonyl products observed from the photolysis of toluene oxide, the modeling performed here does not lend weight to that interpretation. Except at very short (experimentally inaccessible) time scales, the cresol population was always observed to be greater than that of the ketone intermediates, typically by at least 1 order of magnitude. Thus the observed ketene and carbonyl spectra are likely to originate in other species not identified in paper 1, possibly ring-opened products of the species included in the reaction scheme investigated in this work or products of O_2 addition.

References and Notes

(1) Atkinson, R. *Atmos. Environ.* **2000**, *34*, 2063.
(2) Derwent, R. G.; Jenkin, M. E.; Saunders, S. M. *Atmos. Environ.* **1996**, *30*, 181.
(3) Klotz, B.; Barnes, I.; Golding, B. T.; Becker, K.-H. *Phys. Chem. Chem. Phys.* **2000**, *2*, 227.
(4) Suh, I.; Zhang, D.; Zhang, R.; Molina, L. T.; Molina, M. J. *Chem. Phys. Lett.* **2002**, *364*, 454.
(5) Xiao, H.; Zhu, B. *Water Air Soil Pollut.* **2003**, *145*, 3.
(6) Bloss, C.; Wagner, V.; Bonzanini, A.; Jenkin, M. E.; Wirtz, K.; Martin-Reviejo, M.; Pilling, M. J. *Atmos. Chem. Phys.* **2005**, *5*, 623.
(7) Frankcombe, T. J.; Smith, S. C. *J. Phys. Chem. A* **2006**, *111*, 3686.
(8) García-Cruz, I.; Castro, M.; Vivier-Bunge, A. *J. Comput. Chem.* **2000**, *21*, 716.
(9) Huang, M.; Zhang, W.; Yang, Y.; Wang, Z.; Hao, L.; Zhao, W.; Zhao, W.; Li, J.; Gao, X. *J. Mol. Struct. (THEOCHEM)* **2006**, *774*, 1.
(10) Suh, I.; Zhang, R.; Molina, L. T.; Molina, M. J. *J. Am. Chem. Soc.* **2003**, *125*, 12655.
(11) Uc, V. H.; García-Cruz, I.; Hernández-Laguna, A.; Vivier-Bunge, A. *J. Phys. Chem. A* **2000**, *104*, 7847.
(12) Frankcombe, T. J.; Smith, S. C.; Gates, K. E.; Robertson, S. H. *Phys. Chem. Chem. Phys.* **2000**, *2*, 793.
(13) Frankcombe, T. J.; Smith, S. C. *Faraday Discuss.* **2002**, *119*, 159.
(14) Frankcombe, T. J.; Smith, S. C. *J. Theor. Comput. Chem.* **2003**, *2*, 179.
(15) Frankcombe, T. J.; Smith, S. C. *J. Chem. Phys.* **2003**, *119*, 12729.
(16) Frankcombe, T. J.; Smith, S. C. *J. Chem. Phys.* **2003**, *119*, 12741.
(17) Gilbert, R. G.; Smith, S. C. *Theory of Unimolecular and Recombination Reactions*; Blackwell Scientific: Oxford, U.K., 1990.
(18) Lenzer, T.; Luther, K.; Hold, U.; Symonds, A. C. *Springer Proc. Phys.* **1992**, *68*, 237.
(19) Lenzer, T.; Luther, K.; Reihs, K.; Symonds, A. C. *J. Chem. Phys.* **2000**, *112*, 4090.
(20) Nordholm, S.; Schranz, H. W. In *Advances in Chemical Kinetics and Dynamics*; Barker, J. R., Ed.; JAI: Greenwich, U.K., 1995; Vol. 2A, p 245.
(21) Hippler, H.; Troe, J.; Wendelken, H. J. *J. Chem. Phys.* **1983**, *78*, 6709.
(22) Holbrook, K. A.; Pilling, M. J.; Robertson, S. H. *Unimolecular Reactions*, 2nd ed.; John Wiley & Sons: Chichester, U.K., 1996.
(23) Miller, J. A.; Klippenstein, S. J. *J. Phys. Chem. A* **2006**, *110*, 10528.
(24) Gates, K. E.; Robertson, S. H.; Smith, S. C.; Pilling, M. J.; Beasley, M. S.; Maschhoff, K. J. *J. Phys. Chem. A* **1997**, *101*, 5765.
(25) Green, N. J. B.; Robertson, S. H.; Pilling, M. J. *J. Chem. Phys.* **1994**, *100*, 5259.
(26) Anderson, E.; Bai, Z.; Bischof, C.; Blackford, S.; Demmel, J.; Dongarra, J.; Croz, J. D.; Greenbaum, A.; Hammarling, S.; McKenney, A.; Sorensen, D. *LAPACK Users Guide*, 3rd ed.; SIAM: Philadelphia, 1999.
(27) Hindmarsh, A. C. In *Scientific Computing*; Stepleman, R. S., Ed.; North-Holland: Amsterdam, 1983; p 55.